CrossMark

# Inclusion of an arbitrary polygon with graded eigenstrain in an anisotropic piezoelectric half plane

Q.D. Chen [a], K.Y. Xu [a,*], E. Pan [b,c]

[a] Shanghai Institute of Applied Mathematics and Mechanics, Shanghai Key Laboratory of Mechanics in Energy Engineering, Department of Mechanics, Shanghai University, Shanghai 200072, China
[b] The School of Mechanical Engineering, Zhengzhou University, Zhengzhou, Henan 450001, China
[c] Department of Civil Engineering, The University of Akron, OH 44325-3905, USA

ABSTRACT

This paper presents an exact closed-form solution for the Eshelby problem of a polygonal inclusion with graded eigenstrains in an anisotropic piezoelectric half plane with traction-free on its surface. Using the line-source Green's function, the line integral is carried out analytically for the linear eigenstrain case, with the final expression involving only elementary functions. The solutions are applied to the semiconductor quantum wire (QWR) of square, triangular, and rectangular shapes, with results clearly illustrating various influencing factors on the induced fields. The exact closed-form solution should be useful to the analysis of nanoscale QWR structures where large strain and electric fields could be induced by the non-uniform misfit strain.

© 2013 Elsevier Ltd. All rights reserved.

## 1. Introduction

Eshelby problem (Eshelby, 1957, 1961) has been an interesting topic in various engineering and material fields for more than 50 years, and is the subject of constant studies (Willis, 1981; Mura, 1987). Some of the previous studies include the effective elastoplastic behavior of composites (Ju and Sun, 2001), and dynamic Eshelby tensor of ellipsoidal inclusions (Michelitsch et al., 2003), among others. Although most Eshelby problems in isotropic elasticity can be solved analytically for both two-dimensional (2D) and three-dimensional (3D) deformations (see, e.g. Kouris and Mura, 1989), solution to the corresponding anisotropic elasticity is still a challenging and attractive topic. For a transversely isotropic elasticity problem an analytical solution can be obtained (Yu et al., 1994), whilst in an anisotropic elasticity it is usually solved numerically (Dong et al., 2003). As a typical application of the Eshelby solution, it is effective to study the semiconductor properties for efficient device design. However, different from simple isotropic elastic materials, most semiconductor materials show both anisotropic and piezoelectric properties, with some of them being strongly electromechanically coupled (Pan, 2002). For piezoelectric Eshelby inclusion problems, most reported analytical solutions concerned with elliptical/ellipsoidal shapes only (Wang, 1992; Chung and Ting, 1996). In real applications, however, the

Eshelby problem with arbitrarily shaped inclusion is particularly useful in the study of the strained semiconductor quantum devices (Freund and Gosling, 1995; Andreev et al., 1999). In the work of Ru (1999), analytical solutions for Eshelby inclusion of arbitrary shape were derived based on the conformal mapping which maps the exterior of a unit circle onto the exterior of the inclusion. This method is elegant and convenient for the inclusion with smooth boundary. In the work of Pan (2004), the Green's function solutions were adopted with the final solution involving only elementary functions, which is particularly suited for a polygonal inclusion. The perturbation method can also be applied to handle the elastic material anisotropy and arbitrary shape of an inclusion (Wang and Chu, 2006). Zou et al. (2011) applied the extended Stroh formalism to an Eshelby problem of 2D arbitrarily shaped piezoelectric inclusion, which is actually very powerful in treating 2D anisotropic problems. Inclusion of an arbitrary shape with uniform eigenstrains in magnetoelectroelastic bimaterial planes was also investigated (Jiang and Pan, 2004; Zou and Pan, 2012).

We point out that in most of the previous studies, the eigenstrain within the inclusion was assumed to be uniform, which could be very limited because in most semiconductor materials, the eigenstrain shows non-uniform distribution. Thus, the effect of non-uniform eigenstrain on the induced field is particularly interesting. Eshelby (1961) showed that if the eigenstrain inside an ellipsoidal inclusion in an infinite domain is in the form of a polynomial, then the induced-strain field in the inclusion is also characterized by a polynomial of the same order. Other types of

non-uniform eigenstrain were also considered, including an ellipsoidal inclusion with dilatational Gaussian and exponential eigenstrains (Sharma and Sharma, 2003), and an ellipsoidal or elliptic inclusion with linear and polynomial distributions of eigenstrain (Rahman, 2002; Nie et al., 2007; Guo et al., 2011). Recently, Sun et al. (2012) solved the Eshelby inclusion problem of an arbitrary polygon with a linear eigenstrain in an anisotropic piezoelectric full plane via the Green's function method.

In most engineering applications, the size of the substrate would be finite. Liu (2010) studied the 2D periodic inclusion problem in a finite cell and obtained the solution to the problem in terms of Cauchy-type integrals. Using the Somigliana's identity and Green's functions in classical elasticity, analytical solution of the Eshelby tensors of a spherical inclusion embedded concentrically within a finite sphere can be derived (Li et al., 2007). Mejak (2011) obtained the Eshelby tensors for a spherical inclusion within a finite spherical body by power series approximation. Ma and Gao (2011) extended the classical elasticity to strain gradient elasticity theory. Zou et al. (2012) proposed a general approach based on the principle of superposition to study the problem of a finite elastic body with an arbitrarily shaped inclusion. Although the half-plane piezoelectric problem of an arbitrarily shaped inclusion was investigated before (Ru, 2003; Wang and Pan, 2010), solution to the inclusion problem with non-uniform eigenstrain in an anisotropic piezoelectric half plane remains to be solved.

In this paper, an exact closed-form solution for an arbitrarily shaped polygonal inclusion in an anisotropic piezoelectric half plane is presented, where the eigenstrain within the inclusion can be not only uniform but also graded. Based on the equivalent body force and by means of subdomain division, the eigenstrain can be expressed as a linear graded function in every subregion. Thus, we can express the induced elastic and piezoelectric fields in terms of a line integral on the boundary of the inclusion, with the integrand being the multiplication of the line-source Green's function and the equivalent body force of the piezoelectric solid. The line integral can be carried out analytically assuming that the inclusion is a polygon. The most remarkable feature is that the final exact closed-form solution involves only elementary functions, similar to the corresponding isotropic elastic solutions (Faux et al., 1997; Nozaki and Taya, 1997; Glas, 2002a). Using our present simple solutions, the piezoelectric field due to multiple inclusions or an array of QWRs can be easily obtained by adding the contributions from all the QWRs. As numerical examples, our solution is applied to square, triangular, and rectangular QWRs within a GaAs (001) half-plane substrate. Our numerical results clearly show the obvious effects of graded eigenstrain distribution, depth, and orientation of the embedded inclusion on the induced fields. When a QWR is embedded sufficiently deep, our results reduce to the exact closed-form solutions in a full plane (Sun et al., 2012). Furthermore, the piezoelectric field due to an elliptical inclusion can be calculated by an inscribed polygon with a relatively large side number and thus it should be an efficient and recommended method for the elastic and electric field analysis in nanoscale QWR structures.

This paper is organized as follows: In Section 2, we derive an exact closed-form solution in a piezoelectric half plane for a general polygon under a linear eigenstrain in x and z. In Section 3, we apply our solutions to a couple of inclusion problems within a piezoelectric half-plane substrate with traction-free boundary conditions. The effect of different non-uniform eigenstrains, different orientations of the polygon, and different embedded depths of the QWR, along with certain interesting features in the induced fields are discussed. Conclusions are drawn in Section 4.

## 2. Solutions of inclusion problems in piezoelectric half-plane

Let us assume that there is a general inclusion with arbitrary shape in an anisotropic piezoelectric half-plane ($z < 0$), and an extended general eigenstrain $\gamma_{Ij}^*$ (i.e., the eigenstrain $\gamma_{ij}^*$ and eigen-electric field $E_j^*$) within the domain $V$ bounded by its boundary $\partial V$ (Fig. 1). The eigenstrain is further assumed to be a linear function of the coordinates $(x,z)$. Our task is to find the eigenstrain-induced field within and outside the QWR.

For a general eigenstrain $\gamma_{Ij}^*$ at $\mathbf{x} = (x,z)$ within the domain $V$, the induced extended displacement at $\mathbf{X} = (X,Z)$ can be expressed based on the method of superposition and equivalent body-force concept. In other words, the response is an integral, over $V$, of the equivalent body force in the square bracket below, multiplied by the line-source Green's function (Pan, 2004), i.e.,

$$u_K(\mathbf{X}) = -\int_V u_J^K(\mathbf{x};\mathbf{X})[C_{iJLm}\gamma_{Lm}^*(\mathbf{x})]_{,i}dV(\mathbf{x}) \tag{1}$$

where $u_J^K(\mathbf{x};\mathbf{X})$ is the $J$-th Green's elastic displacement/electric potential at $\mathbf{x}$ due to a line-force/line-charge in the $K$-th direction applied at $\mathbf{X}$. Summation is assumed for repeated lowercase (from 1 to 3) and uppercase (from 1 to 4) indices.

Integrating by parts and noticing that the eigenstrain is nonzero only in $V$, Eq. (1) can be written alternatively as

$$u_K(\mathbf{X}) = \int_V u_{J,x_i}^K(\mathbf{x};\mathbf{X})C_{iJLm}\gamma_{Lm}^*(\mathbf{x})dV(\mathbf{x}) \tag{2}$$

Since the eigenstrain can be expressed as a linear function of the coordinates $(x,z)$ (Sun et al., 2012):

$$\gamma_{Lm}^*(\mathbf{x}) = \gamma_{Lm}^{*0} + \gamma_{Lm}^{*x}x + \gamma_{Lm}^{*z}z \tag{3}$$

Eq. (2) becomes

$$u_K(\mathbf{X}) = \int_V u_{J,x_i}^K(\mathbf{x};\mathbf{X})C_{iJLm}[\gamma_{Lm}^{*0} + \gamma_{Lm}^{*x}x + \gamma_{Lm}^{*z}z]dV(\mathbf{x}) \tag{4}$$

or

$$u_K^0(\mathbf{X}) + u_K^x(\mathbf{X}) + u_K^z(\mathbf{X}) \equiv \int_V u_{J,x_i}^K(\mathbf{x};\mathbf{X})[C_{iJLm}\gamma_{Lm}^{*0} + C_{iJLm}\gamma_{Lm}^{*x}x + C_{iJLm}\gamma_{Lm}^{*z}z]dV(x) \tag{5}$$

The involved area integrals can be easily transformed to the line integrals along the boundary of the QWR by the Green formula:

$$u_K^0(\mathbf{X}) = C_{iJLm}\gamma_{Lm}^{*0}\int_{\partial V} u_J^K(\mathbf{x};\mathbf{X})n_i(\mathbf{x})dS(\mathbf{x}) \tag{6}$$
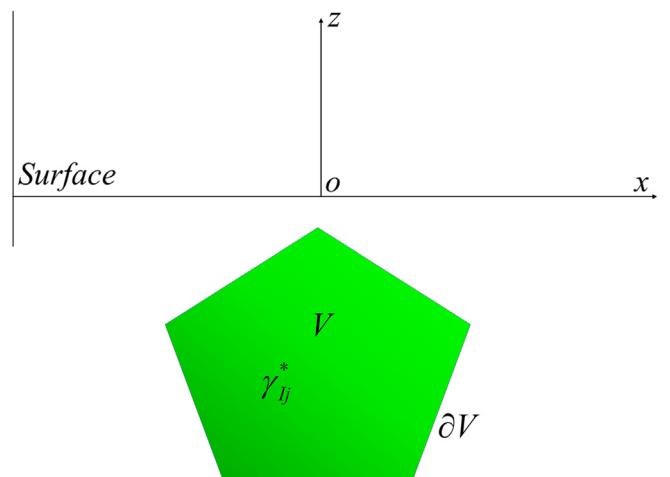


**Fig. 1.** A general inclusion problem in an anisotropic piezoelectric half-plane ($z < 0$): a linear eigenstrain $\gamma_{Ij}^*$ ($\gamma_{ij}^*$ and $-E_j^*$) within an arbitrarily shaped polygon.

$$u_K^x(\boldsymbol{X}) = C_{ijLm}\gamma_{Lm}^{*x}\int_{\partial V}u_J^K(\boldsymbol{x};\boldsymbol{X})xn_i(\boldsymbol{x})dS(\boldsymbol{x}) - C_{xjLm}\gamma_{Lm}^{*x}$$
$$\times \int_{\partial V}U_J^{xK}(\boldsymbol{x};\boldsymbol{X})n_x(\boldsymbol{x})dS(\boldsymbol{x}) \qquad (7)$$

$$u_K^z(\boldsymbol{X}) = C_{ijLm}\gamma_{Lm}^{*z}\int_{\partial V}u_J^K(\boldsymbol{x};\boldsymbol{X})zn_i(\boldsymbol{x})dS(\boldsymbol{x}) - C_{zjLm}\gamma_{Lm}^{*z}$$
$$\times \int_{\partial V}U_J^{zK}(\boldsymbol{x};\boldsymbol{X})n_z(\boldsymbol{x})dS(\boldsymbol{x}) \qquad (8)$$

In Eqs. (7) and (8), the two new functions are defined as

$$U_J^{xK}(\boldsymbol{x};\boldsymbol{X})_{,x} = u_J^K(\boldsymbol{x};\boldsymbol{X})$$
$$U_J^{zK}(\boldsymbol{x};\boldsymbol{X})_{,z} = u_J^K(\boldsymbol{x};\boldsymbol{X}) \qquad (9)$$

Thus, the following four analytical integrations are required in order to find the induced elastic displacement and electric potential.

$$I_x = \int_{\partial V}u_J^K(\boldsymbol{x};\boldsymbol{X})xn_i(\boldsymbol{x})dS(\boldsymbol{x}); \quad I_z = \int_{\partial V}u_J^K(\boldsymbol{x};\boldsymbol{X})zn_i(\boldsymbol{x})dS(\boldsymbol{x})$$
$$J_x = \int_{\partial V}U_J^{xK}(\boldsymbol{x};\boldsymbol{X})n_x(\boldsymbol{x})dS(\boldsymbol{x}); \quad J_z = \int_{\partial V}U_J^{zK}(\boldsymbol{x};\boldsymbol{X})n_z(\boldsymbol{x})dS(\boldsymbol{x}) \qquad (10)$$

It is noted that these four quantities are also functions of the indices $J$ and $K$.

To carry out the integration, we assume as before that the boundary of the linear eigenstrain domain is composed of piecewise straight line segments. We then define an arbitrary line segment in the $(x,z)$-plane starting from point 1 $(x_1,z_1)$ and ending at point 2 $(x_2,z_2)$, in terms of parameter $t$ $(0 \leqslant t \leqslant 1)$, as

$$x = x_1 + (x_2 - x_1)t$$
$$z = z_1 + (z_2 - z_1)t \qquad (11)$$

Then, the outward normal component $n_i(\boldsymbol{x})$ along the line segment is constant, given by

$$n_x = (z_2 - z_1)/l; \quad n_z = -(x_2 - x_1)/l \qquad (12)$$

where $l = \sqrt{(x_2 - x_1)^2 + (z_2 - z_1)^2}$ is the length of the line segment.

Using the exact closed-form expression for the Green's function in a piezoelectric half-plane substrate, the integration along the line segment for $I_x$ can be easily carried out as

$$I_x(\boldsymbol{X}) = n_i\frac{l}{\pi}\mathrm{Im}\left\{A_{JR}h_R^x(X,Z)A_{KR} + \sum_{v=1}^{4}A_{JR}g_R^{xv}(X,Z)Q_{RK}^v\right\} \qquad (13)$$

where the first term involving $h_R^x$ is the contribution from the full-plane Green's function (Sun et al., 2012), the second term involving $g_R^{xv}$ comes from the complementary part, which is used to satisfy the boundary conditions on the surface of the half plane. $Q_{RK}^v$ is related to the boundary conditions on the surface of the half plane. Also in Eq. (13), summation from 1 to 4 is implied for the repeated index $R$. Since the first term on the right-hand side of Eq. (13) has been determined previously (Sun et al., 2012), we only need to discuss the second term in Eq. (13).

The function $g_R^{xv}(X,Z)$ and its derivatives (required for the induced strain calculation) are given below:

$$g_R^{xv}(X,Z) = \int_0^1 \ln(z_R - \bar{s}_v)xdt$$
$$= \frac{x_2 - x_1}{4a^2}\left[a(2c - a) - 2(c^2 - a^2)\ln(a + c) + 2c^2\ln(c)\right]$$
$$+ \frac{x_1}{a}\left[-a + (a + c)\ln(a + c) - c\ln(c)\right] \qquad (14)$$

$$\frac{\partial g_R^{xv}(X,Z)}{\partial X} = -\frac{x_2 - x_1}{a^2}\left[a - c\ln\left(\frac{a+c}{c}\right)\right] - \frac{x_1}{a}\ln\left(\frac{a+c}{c}\right)$$
$$\frac{\partial g_R^{xv}(X,Z)}{\partial Z} = -\frac{(x_2 - x_1)\bar{p}_v}{a^2}\left[a - c\ln\left(\frac{a+c}{c}\right)\right] - \frac{x_1\bar{p}_v}{a}\ln\left(\frac{a+c}{c}\right) \qquad (15)$$

where

$$a = (x_2 - x_1) + p_R(z_2 - z_1)$$
$$c = (x_1 + p_Rz_1) - \bar{s}_v \qquad (16)$$

with the overbar on $s_v$ $(\equiv X + p_vZ)$ denoting the complex conjugate and $p_v$ being the Stroh eigenvalue.

Similarly for $I_z$, its integration along each line segment can be found as

$$I_z(\boldsymbol{X}) = n_i\frac{l}{\pi}\mathrm{Im}\left\{A_{JR}h_R^z(X,Z)A_{KR} + \sum_{v=1}^{4}A_{JR}g_R^{zv}(X,Z)Q_{RK}^v\right\} \qquad (17)$$

where

$$g_R^{zv}(X,Z) = \int_0^1 \ln(z_R - \bar{s}_v)zdt$$
$$= \frac{z_2 - z_1}{4a^2}\left[a(2c - a) - 2(c^2 - a^2)\ln(a + c) + 2c^2\ln(c)\right]$$
$$+ \frac{z_1}{a}\left[-a + (a + c)\ln(a + c) - c\ln(c)\right] \qquad (18)$$

$$\frac{\partial g_R^{zv}(X,Z)}{\partial X} = -\frac{z_2 - z_1}{a^2}\left[a - c\ln\left(\frac{a+c}{c}\right)\right] - \frac{z_1}{a}\ln\left(\frac{a+c}{c}\right)$$
$$\frac{\partial g_R^{zv}(X,Z)}{\partial Z} = -\frac{(z_2 - z_1)\bar{p}_v}{a^2}\left[a - c\ln\left(\frac{a+c}{c}\right)\right] - \frac{z_1\bar{p}_v}{a}\ln\left(\frac{a+c}{c}\right) \qquad (19)$$

We now treat the integrations in $J_x$ and $J_z$ along the straight line segment. First, since half-plane Green's function can be expressed as (Pan, 2004)

$$u_J^K(\boldsymbol{x},\boldsymbol{X}) = \frac{1}{\pi}\mathrm{Im}\{A_{JR}\ln(z_R - s_R)A_{KR}\}$$
$$+ \frac{1}{\pi}\mathrm{Im}\sum_{v=1}^{4}\{A_{JR}\ln(z_R - \bar{s}_v)Q_{RK}^v\}$$
$$= \frac{1}{\pi}\mathrm{Im}\{A_{JR}\ln(p_Rz + x - s_R)A_{KR}\}$$
$$+ \frac{1}{\pi}\mathrm{Im}\sum_{v=1}^{4}\{A_{JR}\ln(p_Rz + x - \bar{s}_v)Q_{RK}^v\} \qquad (20)$$

we have, based on Eq. (9),

$$U_J^{xK}(\boldsymbol{x},\boldsymbol{X}) = \frac{1}{\pi}\mathrm{Im}\left\{A_{JR}\left[-x + \frac{b_1\ln(a_1x+b_1)}{a_1} + x\ln(a_1x+b_1)\right]A_{KR}\right\}$$
$$+ \frac{1}{\pi}\mathrm{Im}\sum_{v=1}^{4}\left\{A_{JR}\left[-x + \frac{c_1\ln(a_1x+c_1)}{a_1} + x\ln(a_1x+c_1)\right]Q_{RK}^v\right\} \qquad (21)$$

where

**Table 1**
Stress component $\sigma_{xx}$ (GPa) induced by an elliptical QWR within the GaAs (0 0 1) half plane located at a depth of 20 nm. The eigenstrain inside the ellipse is linear in $x$, i.e., $\gamma_{Lm}^0 = 0, \gamma_{xx}^{*x} = \gamma_{zz}^{*x} = 0.07, \gamma_{Lm}^{*z} = 0$. The ellipse is approximated by $N$-sided polygon ($N = 20, 30, 50, 80, 100$).

| $(X,Z)$ (nm) | $N = 20$ | $N = 30$ | $N = 50$ | $N = 80$ | $N = 100$ |
|---|---|---|---|---|---|
| $(1,-19)$ | −0.24376 | −0.24523 | −0.24443 | −0.24396 | −0.24396 |
| $(2,-18)$ | −0.48637 | −0.48932 | −0.48771 | −0.48678 | −0.48677 |
| $(3,-17)$ | −0.72726 | −0.73165 | −0.72922 | −0.72784 | −0.72781 |
| $(4,-16)$ | −0.96574 | −0.97153 | −0.96827 | −0.96645 | −0.96639 |
| $(5,-15)$ | −1.20093 | −1.20820 | −1.20413 | −1.20191 | −1.20179 |
| $(6,-14)$ | −1.43145 | −1.44086 | −1.43606 | −1.43349 | −1.43324 |
| $(7,-13)$ | −1.65697 | −1.66864 | −1.66347 | −1.66038 | −1.66005 |
| $(8,-12)$ | **−1.88829** | **−1.88472** | **−1.88625** | **−1.88200** | **−1.88140** |
| $(9,-11)$ | **−0.58914** | **−0.58789** | **−0.58546** | **−0.57246** | **−0.58469** |
| $(10,-10)$ | −0.51444 | −0.52481 | −0.51899 | −0.51810 | −0.51964 |
| $(11,-9)$ | −0.48891 | −0.49648 | −0.49452 | −0.49340 | −0.49362 |
| $(12,-8)$ | −0.49381 | −0.49796 | −0.49577 | −0.49466 | −0.49442 |
| $(13,-7)$ | −0.49905 | −0.50222 | −0.49999 | −0.49891 | −0.49861 |
| $(14,-6)$ | −0.49294 | −0.49592 | −0.49385 | −0.49286 | −0.49257 |
| $(15,-5)$ | −0.47410 | −0.47705 | −0.47521 | −0.47430 | −0.47406 |

**Table 2**
Electric displacement component $D_z$ ($\times 10^{-3}$ C/m²) induced by an elliptical QWR within the GaAs (0 0 1) half plane located at a depth of 20 nm. The eigenstrain inside the ellipse is linear in $x$, i.e., $\gamma_{Lm}^{*0}=0, \gamma_{xx}^{*x}=\gamma_{zz}^{*x}=0.07, \gamma_{Lm}^{*z}=0$. The ellipse is approximated by $N$-sided polygon ($N=20, 30, 50, 80, 100$).

| $(X,Z)$ (nm) | $N=20$ | $N=30$ | $N=50$ | $N=80$ | $N=100$ |
|---|---|---|---|---|---|
| $(1,-19)$ | $-1.51122$ | $-1.53484$ | $-1.53737$ | $-1.53677$ | $-1.53763$ |
| $(2,-18)$ | $-1.592$ | $-1.36874$ | $-1.37200$ | $-1.37176$ | $-1.37263$ |
| $(3,-17)$ | $-1.17334$ | $-1.19506$ | $-1.19907$ | $-1.19918$ | $-1.20007$ |
| $(4,-16)$ | $-0.99268$ | $-1.01298$ | $-1.01779$ | $-1.01827$ | $-1.01915$ |
| $(5,-15)$ | $-0.80321$ | $-0.82185$ | $-0.82767$ | $-0.82849$ | $-0.82934$ |
| $(6,-14)$ | $-0.60499$ | $-0.62169$ | $-0.62863$ | $-0.62960$ | $-0.63048$ |
| $(7,-13)$ | $-0.40534$ | $-0.41218$ | $-0.42150$ | $-0.42168$ | $-0.42307$ |
| $\mathbf{(8,-12)}$ | $\mathbf{-0.22147}$ | $\mathbf{-0.19260}$ | $\mathbf{-0.20866}$ | $\mathbf{-0.20585}$ | $\mathbf{-0.20818}$ |
| $\mathbf{(9,-11)}$ | $\mathbf{1.00050}$ | $\mathbf{1.09223}$ | $\mathbf{0.98785}$ | $\mathbf{1.00355}$ | $\mathbf{1.02727}$ |
| $(10,-10)$ | $1.13329$ | $1.17148$ | $1.16240$ | $1.16108$ | $1.15918$ |
| $(11,-9)$ | $1.25572$ | $1.27116$ | $1.26385$ | $1.26203$ | $1.26033$ |
| $(12,-8)$ | $1.25870$ | $1.27339$ | $1.26947$ | $1.26806$ | $1.26730$ |
| $(13,-7)$ | $1.18310$ | $1.19768$ | $1.19577$ | $1.19475$ | $1.19450$ |
| $(14,-6)$ | $1.06612$ | $1.07958$ | $1.07868$ | $1.07787$ | $1.07787$ |
| $(15,-5)$ | $0.92930$ | $0.94106$ | $0.94056$ | $0.93987$ | $0.93997$ |

$$a_1 = 1$$
$$b_1 = p_R z - s_R \tag{22}$$
$$c_1 = p_R z - \bar{s}_v$$

Similarly, we have

$$U_J^{zK}(\boldsymbol{x},\boldsymbol{X}) = \frac{1}{\pi}\mathrm{Im}\left\{A_{JR}\left[-z + \frac{b_2\ln(a_2 z + b_2)}{a_2} + z\ln(a_2 z + b_2)\right]A_{KR}\right\}$$
$$+\frac{1}{\pi}\mathrm{Im}\sum_{v=1}^{4}\left\{A_{JR}\left[-z + \frac{c_2\ln(a_2 z + c_2)}{a_2} + z\ln(a_2 z + c_2)\right]Q_{RK}^{v}\right\} \tag{23}$$

with

$$a_2 = p_R$$
$$b_2 = x - s_R \tag{24}$$
$$c_2 = x - \bar{s}_v$$

Integration of (21) and (23) gives us

$$J_x(\boldsymbol{X}) = n_x\frac{l}{\pi}\mathrm{Im}\left\{A_{JR}H_R^x(X,Z)A_{KR} + \sum_{v=1}^{4}A_{JR}G_R^{xv}(X,Z)Q_{RK}^{v}\right\} \tag{25}$$

$$J_z(\boldsymbol{X}) = n_z\frac{l}{\pi}\mathrm{Im}\left\{A_{JR}H_R^z(X,Z)A_{KR} + \sum_{v=1}^{4}A_{JR}G_R^{zv}(X,Z)Q_{RK}^{v}\right\} \tag{26}$$

in which the terms $H_R^x$ and $H_R^z$ were derived previously (Sun et al., 2012). We thus need to calculate only the functions $G_R^{xv}(X,Z)$, $G_R^{zv}(X,Z)$ and their derivatives. They are

$$G_R^{xv}(X,Z) = \int_0^1\left[-x + \frac{c_1\ln(a_1 x + c_1)}{a_1} + x\ln(a_1 x + c_1)\right]dt$$
$$= -\frac{x_2 + x_1}{2}$$
$$+\frac{1}{4a}\left[2ac - a^2 - 2(c^2 - a^2)\ln(a + c) + 2c^2\ln(c)\right] + \frac{c}{a}$$
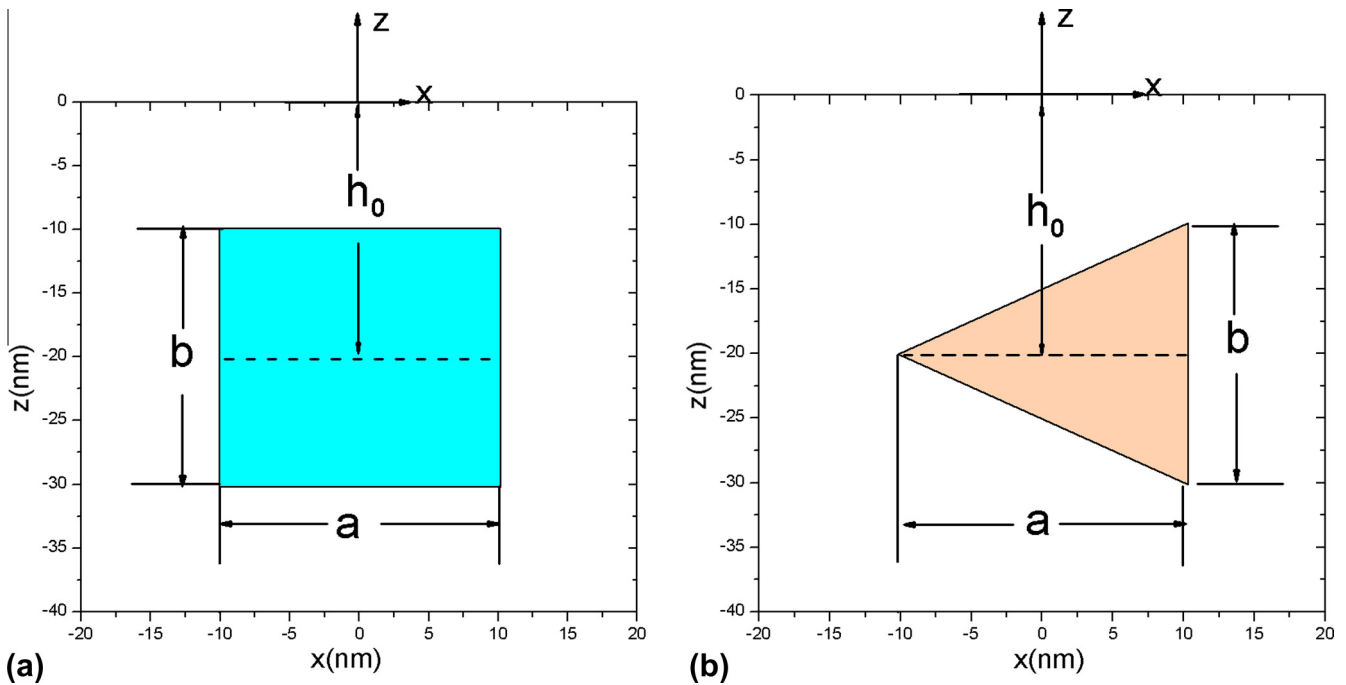$$\times\left[-a + (a + c)\ln(a + c) - c\ln(c)\right] \tag{27}$$

and

$$\frac{\partial G_R^{xv}(X,Z)}{\partial X} = -\frac{1}{a}\left\{a\ln(a + c) + c\ln\left(\frac{a+c}{c}\right) - c\right\}$$
$$\frac{\partial G_R^{xv}(X,Z)}{\partial Z} = -\frac{\bar{p}_v}{a}\left\{a\ln(a + c) + c\ln\left(\frac{a+c}{c}\right) - c\right\} \tag{28}$$

Similarly, we have

$$G_R^{zv}(X,Z) = \int_0^1\left[-z + \frac{c_2\ln(a_2 z + c_2)}{a_2} + z\ln(a_2 z + c_2)\right]dt$$
$$= -\frac{z_2 + z_1}{2}$$
$$+\frac{1}{4ap_R}\left[2ac - a^2 - 2(c^2 - a^2)\ln(a + c) + 2c^2\ln(c)\right]$$
$$+\frac{c}{ap_R}\left[-a + (a + c)\ln(a + c) - c\ln(c)\right] \tag{29}$$

$$\frac{\partial G_R^{zv}(X,Z)}{\partial X} = -\frac{1}{ap_R}\left\{a\ln(a + c) + c\ln\left(\frac{a+c}{c}\right) - c\right\}$$
$$\frac{\partial G_R^{zv}(X,Z)}{\partial Z} = -\frac{\bar{p}_v}{ap_R}\left\{a\ln(a + c) + c\ln\left(\frac{a+c}{c}\right) - c\right\} \tag{30}$$



**Fig. 2.** A square QWR (a) and a triangle QWR (b) within a half-plane substrate ($z < 0$).

With the extended displacements and their derivatives, we can find immediately the elastic strain and electric fields using the following expressions

$$\gamma_{kp}(\boldsymbol{X}) = \frac{1}{2}\gamma_{Lm}^{*}C_{ijLm}\int_{\partial V}\left[u_{J,X_p}^{k}(\boldsymbol{x};\boldsymbol{X}) + u_{J,X_k}^{p}(\boldsymbol{x};\boldsymbol{X})\right]n_i(\boldsymbol{x})dS(\boldsymbol{x}); \quad k,p = 1,2,3 \quad (31a)$$

$$E_p(\boldsymbol{X}) = -\gamma_{Lm}^{*}C_{ijLm}\int_{\partial V}u_{J,X_p}^{4}(\boldsymbol{x};\boldsymbol{X})\,n_i(\boldsymbol{x})dS(\boldsymbol{x}); \quad p = 1,2,3 \quad (31b)$$

The stresses and electric displacements can be obtained from the strain and electric fields via the coupled constitutive relation.

In summary, we have derived the exact closed-form solutions for the piezoelectric fields induced by an arbitrary polygonal inclusion in an anisotropic piezoelectric half plane. Since our result is in an exact closed form, solution to multiple inclusions can be simply derived by superposing the contributions from all inclusions. This is particularly useful in analyzing the induced piezoelectric fields in QWR array (Glas, 2002a,b). Furthermore, a solution to the inclusion with curved boundary can also be obtained by approximating the curved boundary with piecewise straight-line segments. It is worth emphasizing that our results include the uniform eigenstrain case in a general anisotropic piezoelectric half-plane substrate (Pan, 2004) as the special case.

## 3. Numerical examples

We assume that there is an elliptical QWR with its semi-major axis $a = 20$ nm along the $x$-direction and semi-minor axis $b = 10$ nm along the $z$-direction in a GaAs (001) half plane. The vertical distance of the QWR to the surface of the half plane is $h_0$. Within the ellipse there is a linear eigenstrain distribution in $x$, i.e., $\gamma_{Lm}^{*0} = 0, \gamma_{xx}^{*x} = \gamma_{zz}^{*x} = 0.07, \gamma_{Lm}^{*z} = 0$. The elastic properties of GaAs (001) are $C_{11} = 118 \times 10^9$ N/m², $C_{12} = 54 \times 10^9$ N/m², and $C_{44} = 59 \times 10^9$ N/m². The piezoelectric constant and relative permeability are, respectively, $e_{14} = -0.16$ C/m² and $\varepsilon_r = 12.5$. We point out that, for GaAs (001), the global coordinates $x$, $y$, and $z$ are coincident with the crystalline axes [100], [010], and [001]. In our calculation, we approximate the curved ellipse with $N$ piecewise straight line segments. Namely, we replace the ellipse with an $N$-sided regular polygon, for $N$ equals 20, 30, 50, 80, and 100. The induced stress and electric displacement along the diagonal line of the ellipse ($X = Z + h_0, h_0 = 20$ nm) are listed in Tables 1 and 2 for the polygon with different side $N$. Notice that points from $(1, -19)$ to $(8, -13)$ are inside the elliptical QWR, whilst points from $(9, -12)$ to $(15, -5)$ are in the half-plane substrate.

Tables 1 and 2 show the induced fields within the ellipse and in the half-plane substrate. It is noticed that these quantities converge with increasing $N$. It is further noticed that the stress and electric
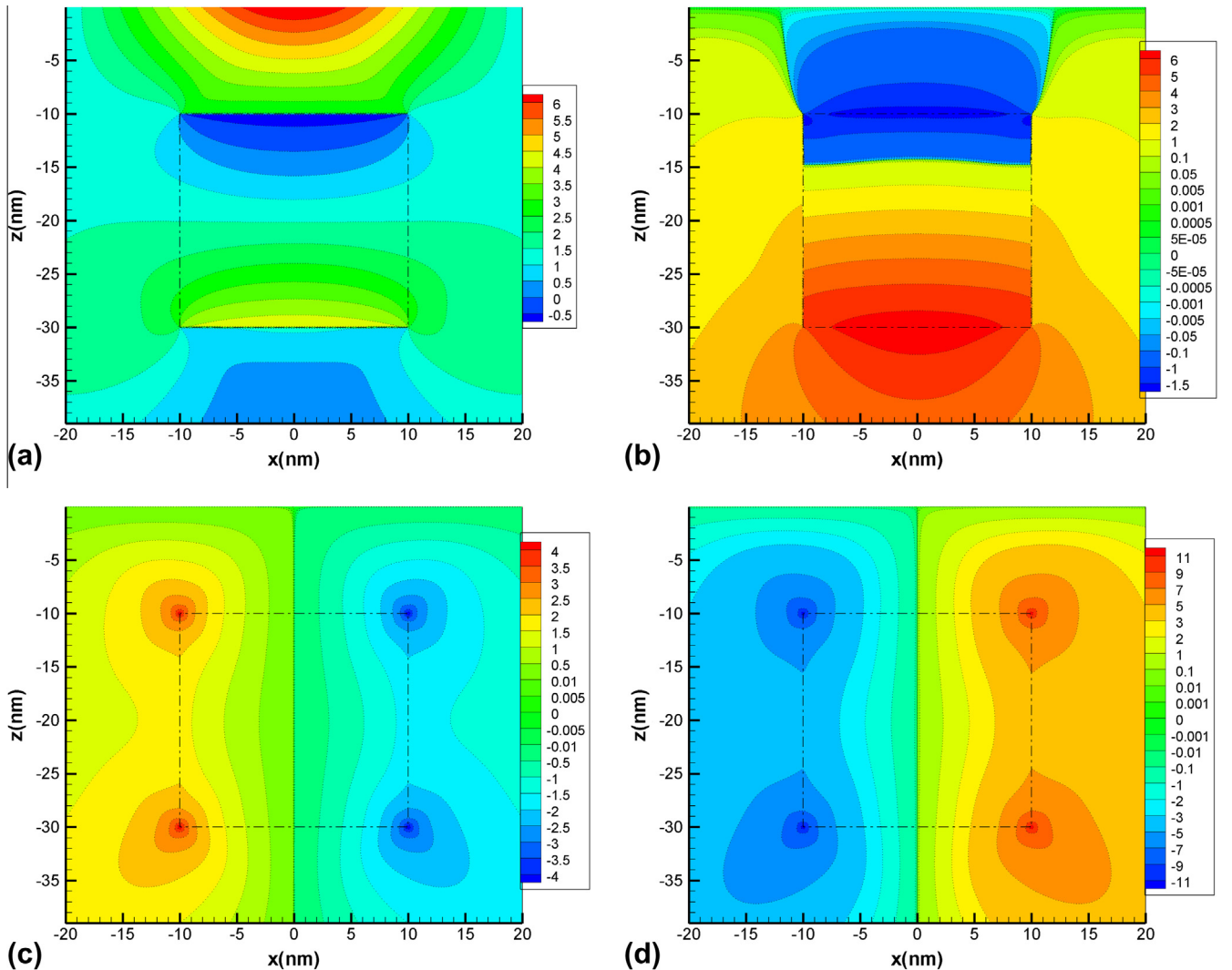


**Fig. 3.** A square QWR with eigenstrain $\gamma_{Lm}^{*0} = 0, \gamma_{Lm}^{*x} = 0, \gamma_{xx}^{*z} = \gamma_{zz}^{*z} = 0.07$ in the GaAs (001) half-plane substrate: (a) contours of stress $\sigma_{xx}$ (GPa); (b) contours of stress $\sigma_{zz}$ (GPa); (c) contours of stress $\sigma_{xz}$ (GPa); (d) contours of electric displacement $D_z$ ($\times 10^{-3}$ C/m²).

displacement for points near the center converge faster than those far from the center. Also for points close to the interface between the inclusion and substrate, the convergence becomes very slow. It is particularly noted that electric displacement $D_z$ is negative within the elliptical QWR but positive in the substrate. This observation illustrates that a large number of polarization charges concentrate on the interface, i.e., the electric displacement $D_z$ is discontinuous across the interface along the diagonal direction of the inclusion. We have also checked the stresses and electric displacements both in the inclusion and substrate induced by different linear eigenstrain distributions and found that they all converge as $N$ increases.

The exact closed-form solutions can be applied to the QWR made of different shapes with three types of eigenstrain distribution: Case #1 with a linear eigenstrain in $x$ ($\gamma_{Lm}^{*0} = 0, \gamma_{xx}^{*x} = \gamma_{zz}^{*x} = 0.07, \gamma_{Lm}^{*z} = 0$); Case #2 with a linear eigenstrain in $z$ ($\gamma_{Lm}^{*0} = 0, \gamma_{xx}^{*x} = 0, \gamma_{xx}^{*z} = \gamma_{zz}^{*z} = 0.07$); and Case #3 with a linear eigenstrain in both $x$ and $z$ ($\gamma_{Lm}^{*0} = 0, \gamma_{xx}^{*x} = \gamma_{zz}^{*x} = 0.07, \gamma_{xx}^{*z} = \gamma_{zz}^{*z} = 0.07$). A square QWR ($a \times b = 20$ nm $\times 20$ nm) in piezoelectric GaAs (0 0 1) is embedded symmetrically (about the $z$-axis) within the substrate at a depth of 20 nm from the surface as the first numerical example (shown in Fig. 2a). The second numerical example is an isosceles triangular QWR (i.e., the base-line length is $b = 20$ nm and the height is $a = 20$ nm) within the GaAs (0 0 1) substrate (Fig. 2b) located also at a depth of 20 nm below the free surface.

First, to further verify our solutions, we have calculated the induced stresses and electric displacements for the two models under linear eigenstrain in $x$ (Case #1). As compared to the full-plane results (Sun et al., 2012), the induced fields ($\sigma_{zz}, \sigma_{xz}, D_z$) quickly converge to zero when approaching the boundary, satisfying the traction-free conditions (figures not included). On the other hand, our half-plane results approach those in Sun et al. (2012) when the depth approaches infinity.

Fig. 3a–d show the contours of the stress and electric displacement for the square QWR case due to a linear eigenstrain in $z$. We can clearly observe that the distribution of the induced stresses and electric displacements is symmetric with respect to $z$-axis. Comparing to the results in the corresponding full-plane case, we find that the free surface condition not only alters the contour shapes, especially for the regions close to surface, but also increases the magnitude of the induced stress and electric displacement within the inclusion. For instance, in the half-plane case, the stresses $\sigma_{xx}$ and $\sigma_{zz}$ within a square reach their maximums at the bottom side of the square, being, respectively, 4.0 and 6.0 GPa. Compared to the maximum values which appear at the top or bottom side of a square in a full plane, the stresses $\sigma_{xx}$ and $\sigma_{zz}$ increase about 33% and 50%, respectively. It is also observed that the normal stress $\sigma_{xx}$ reaches 6.1 GPa on the free surface, and the stresses $\sigma_{zz}$, $\sigma_{xz}$ and electric displacement $D_z$ are zero on the free surface,
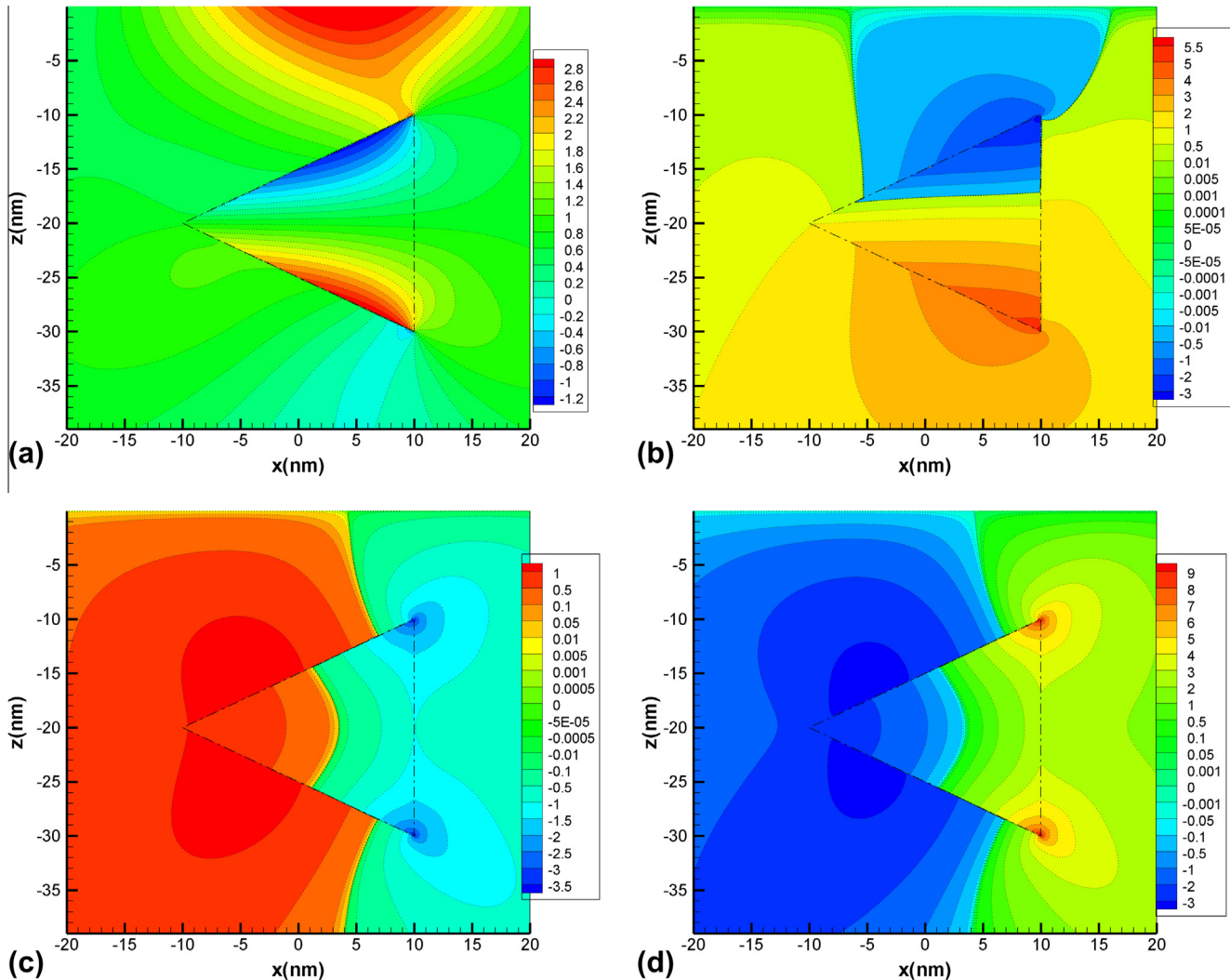


**Fig. 4.** A triangular QWR with eigenstrain $\gamma_{Lm}^{*0} = 0, \gamma_{Lm}^{*x} = 0, \gamma_{xx}^{*z} = \gamma_{zz}^{*z} = 0.07$ in the GaAs (0 0 1) half-plane substrate: (a) contours of stress $\sigma_{xx}$ (GPa); (b) contours of stress $\sigma_{zz}$ (GPa); (c) contours of stress $\sigma_{xz}$ (GPa); (d) contours of electric displacement $D_z$ ($\times 10^{-3}$ C/m²).

satisfying again the given boundary conditions. It is further noted that the contour shapes of the stress $\sigma_{xz}$ and electric displacement $D_z$ are exactly the same except for their magnitudes, with concentrations occurring at the four corners of the square. Therefore, in the fabrication and design of QWR structure, the distance between QWR and free surface needs to be carefully arranged by considering the contour features observed.

Fig. 4a–d shows the contours of the stress and electric displacement induced by a triangular QWR under a hydrostatic linear eigenstrain in z. For this case, it is clear that there is no longer any symmetry in the contours. It can be seen from Fig. 4a that the magnitude of the stress $\sigma_{xx}$ on the free surface is around 2.8 GPa, much less than that for the square QWR case (6.1 GPa). This demonstrates that the induced fields can depend strongly on the QWR shape. It is also interesting to observe that all the induced fields are continuous around the left vertex of the triangle, whilst there exists a singularity at the other two vertices, which will be further investigated later on. We should point out that the stress and electric displacement due to a square or triangular QWR under linear eigenstrains in both x and z (Case #3) can be calculated by simply taking the summation of the induced fields corresponding to the previous two cases (Cases #1 and #2).

We further point out that for the case of multiple QWRs, the induced fields can be obtained by superimposing the contribution from each QWR. For instance, Fig. 5a–d show the contours of the induced fields for three triangular QWRs embedded into GaAs (0 0 1) half-plane substrate, all located at the depth of 20 nm. In our calculation, the eigenstrain within each QWR is linear in z. As shown in Fig. 5a, the magnitude of the stress $\sigma_{xx}$ on the free surface is 4.0 GPa. This value is greater than the value (2.8 GPa) induced by a single triangular QWR. Again, the three field components ($\sigma_{zz}$, $\sigma_{xz}$, $D_z$) satisfy the traction-free boundary conditions. We also remark that, compared to the results due to a single triangular QWR, these figures show clearly the interactive influence of the neighboring QWRs on the induced field.

We now consider a special and interesting case where the average eigenstrain within the QWR is zero. The QWR is embedded in a half plane and we would like to calculate the means of the induced strain and stress fields within the QWR. For the square QWR case under a linear eigenstrain in x (Fig. 2a), we found that the means of strain components ($\bar{\gamma}_{xx}$, $\bar{\gamma}_{zz}$), electric-field components ($\bar{E}_x$, $\bar{E}_z$) and stress components ($\bar{\sigma}_{xx}$, $\bar{\sigma}_{zz}$) are zero, but $\bar{\gamma}_{xz} = 0.0063$, $\bar{\sigma}_{xz} = 0.75$ GPa and electric displacement $\bar{D}_z = -2.02 \times 10^{-3}$ C/m². For a linear eigenstrain in z (actually in $z + h_0$ as shown in Fig. 2a in order that the average eigenstrain is zero within the QWR), the non-zero means of the induced fields are $\bar{\gamma}_{xx} = 0.0064$, $\bar{\gamma}_{zz} = 0.016$, $\bar{\sigma}_{xx} = 1.63$ GPa, $\bar{\sigma}_{zz} = 2.27$ GPa. For an isosceles triangular QWR (Fig. 2b), if a symmetric linear eigenstrain in $z + h_0$ is distributed, then the average eigenstrain within the QWR is zero. The non-zero means of the induced fields are $\bar{\gamma}_{xx} = 0.0026$, $\bar{\gamma}_{zz} = 0.0087$, $\bar{\gamma}_{xz} = -0.0025$, $\bar{\sigma}_{xx} = 0.77$ GPa, $\bar{\sigma}_{zz} = 1.17$ GPa, $\bar{\sigma}_{xz} = -0.31$ GPa, and $\bar{D}_z = 0.81 \times 10^{-3}$ C/m². During our calculations, we also notice that the induced electric fields within the QWR are zero for the GaAs (0 0 1) half-plane case. This phenomenon is actually consistent with previous well-known observation in the superlattice structures (Smith, 1986). These results also illustrate the significant effect of different eigenstrains, QWR shapes, and free surface conditions on the induced piezoelectric fields.

Another interesting issue is on the effect of QWR depth on the induced average fields within the QWR. Besides the two QWR models (square and triangle) presented above, we also consider a thin rectangular QWR ($a \times b = 20$ nm $\times$ 5 nm) located at a depth of 20 nm, with its long side parallel to the x-axis and short side to the z-axis. For easy analysis, we define the dimensionless averages of the stress and electric displacement components as $\bar{\sigma}_{ij}^*$ ($\bar{\sigma}_{ij}/(0.75$ GPa$)$), $\bar{D}_z^*$ ($\bar{D}_z/(-2.02 \times 10^{-3}$ C/m²$)$), respectively. Fig. 6a–d show the variation of the dimensionless averages of the internal fields ($\bar{\sigma}_{xx}^*, \bar{\sigma}_{zz}^*, \bar{\sigma}_{xz}^*, \bar{D}_z^*$) for the three QWR models with different dimensionless depths $h^* = -z/a$ ($h^* > 0.5$). We point out that coordinate $-z$ is the vertical distance from the center of symmetric
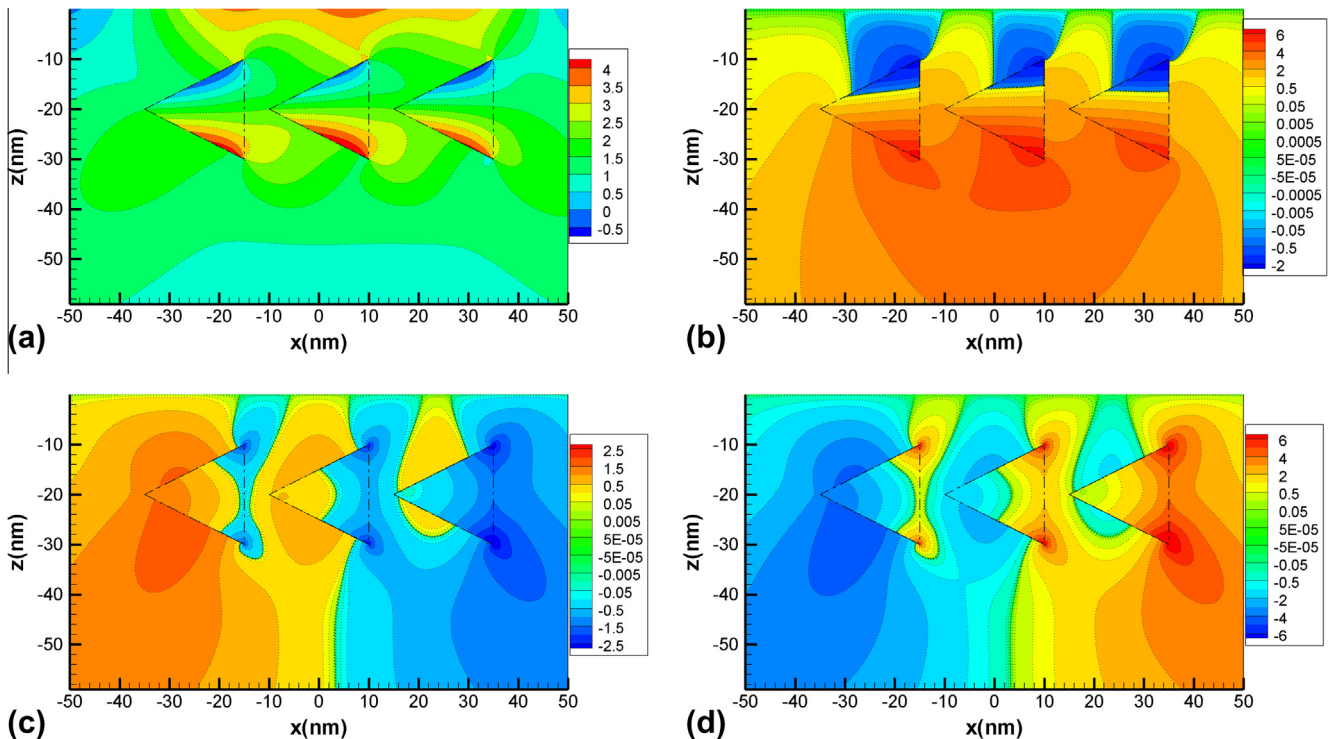


**Fig. 5.** Three triangular QWRs with eigenstrain $\gamma_{Lm}^0 = 0, \gamma_{Lm}^{*x} = 0, \gamma_{xx}^{*z} = \gamma_{zz}^{*z} = 0.07$ in the GaAs (0 0 1) half-plane substrate: (a) contours of stress $\sigma_{xx}$ (GPa); (b) contours of stress $\sigma_{zz}$ (GPa); (c) contours of stress $\sigma_{xz}$ (GPa); (d) contours of electric displacement $D_z$ ($\times 10^{-3}$ C/m²).
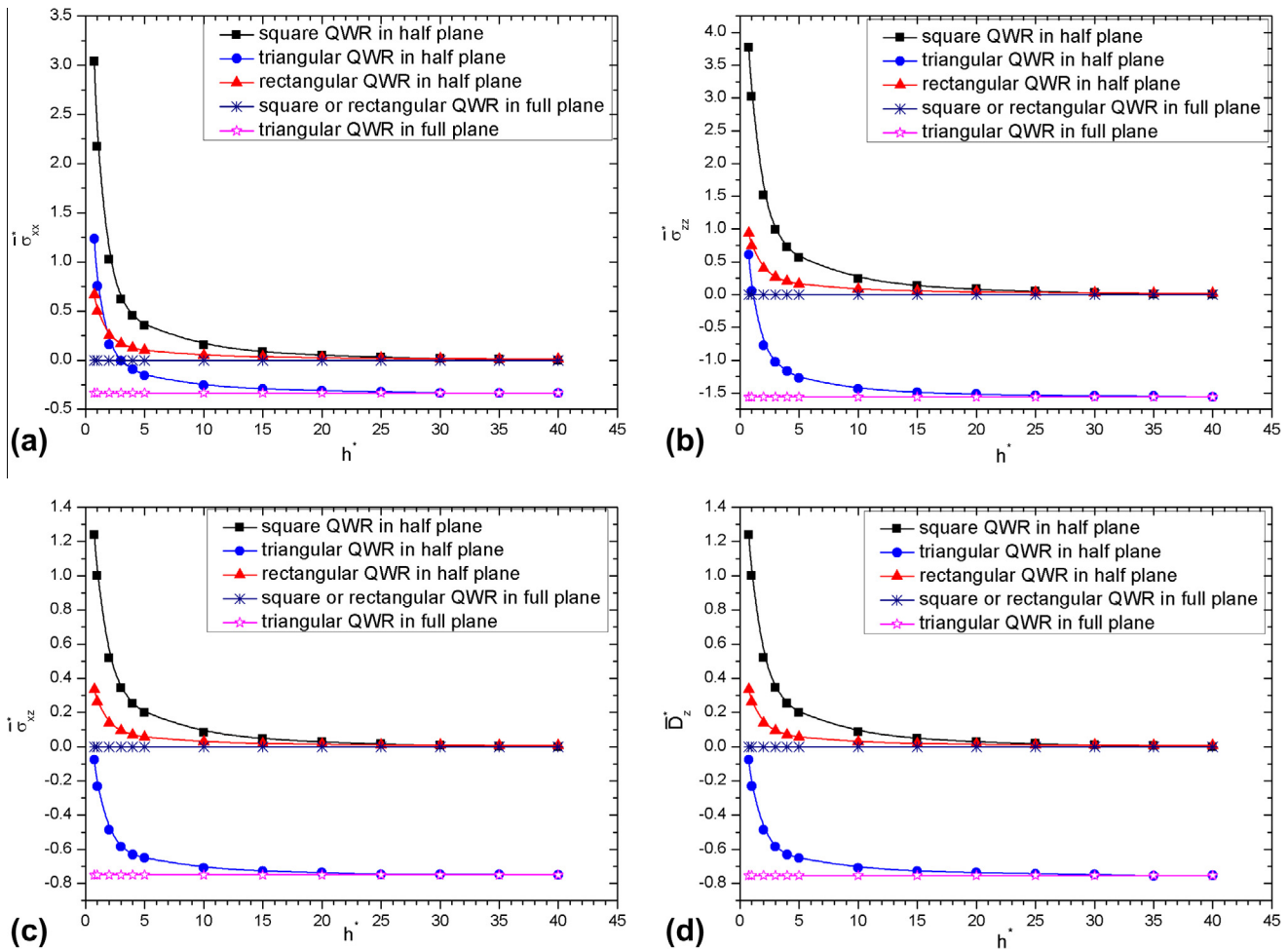
**Fig. 6.** Variation of the dimensionless averages of the stress and electric displacement components induced by a QWR (square, triangle, and rectangle) vs. dimensionless depth $h^*$ under linear eigenstrain $\gamma_{Lm}^{*0} = 0$, $\gamma_{xx}^{*x} = \gamma_{zz}^{*x} = 0.07$, $\gamma_{xx}^{*z} = \gamma_{zz}^{*z} = 0.07$: (a) variation of $\bar{\sigma}_{xx}^*$; (b) variation of $\bar{\sigma}_{zz}^*$; (c) variation of $\bar{\sigma}_{xz}^*$; (d) variation of $\bar{D}_z^*$.
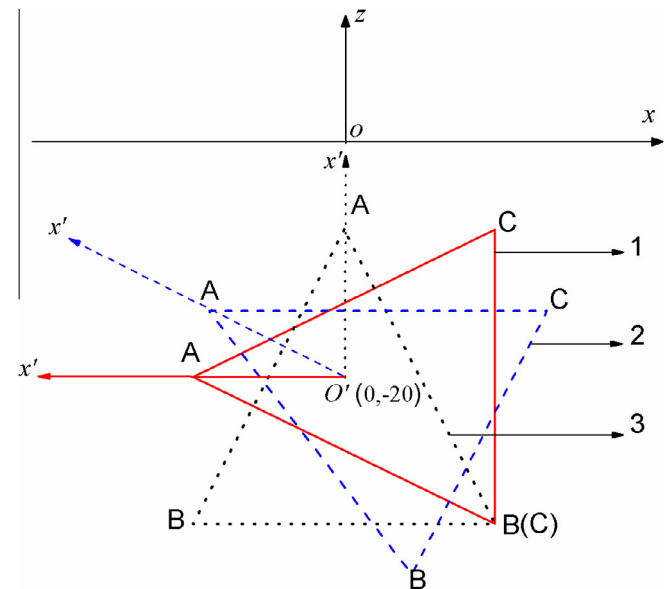


**Fig. 7.** A triangular QWR in three different orientations within the GaAs (001) half-plane substrate.

axis of inclusion to the boundary of the half plane. It can be observed from Fig. 6a–d that these averages all approach the full-plane results with increasing depth. Since these fields converge to the full-plane results, one can define a critical dimensionless depth $h_c^*$ so that the half-plane results can be approximated by those in the corresponding full-plane when $h^* \geqslant h_c^*$. For instance, when the dimensionless depth $h^* \geqslant 20$, the absolute errors of the induced average fields within the QWR between the half- and full-plane are less than 0.05. In other words, for a given absolute error of 0.05, the critical depth can be selected at $h_c^* = 20$ (i.e., the actual embedded depth 400 nm) for these three QWR models in the GaAs (001) half plane.

Finally, we come back to the vertex singularity issue. From Eqs. (15), (19), (28), and (30), we can easily observe that the strain and electric-field components may be of logarithmic singularity at the vertices. For the square model, the contours in Fig. 3c and d show that the shear stress and electric displacement components are singular at the four corners. However, for the triangular QWR, all fields around the left vertex are regular as shown in Fig. 4. This interesting feature motivates us to investigate the effect of the orientation of the triangular QWR on the vertex singularity. Fig. 7 shows a triangular QWR embedded in the half plane at the same depth of $h_0$ (20 nm) but with three different orientations. Fig. 8a(c) and b(d) show the variation of the dimensionless stress $\sigma_{xx}^*$ and electric displacement $D_z^*$ along the local dimensionless coordinate $x'/a$ originated at $O'(0, -20)$ under linear eigenstrain
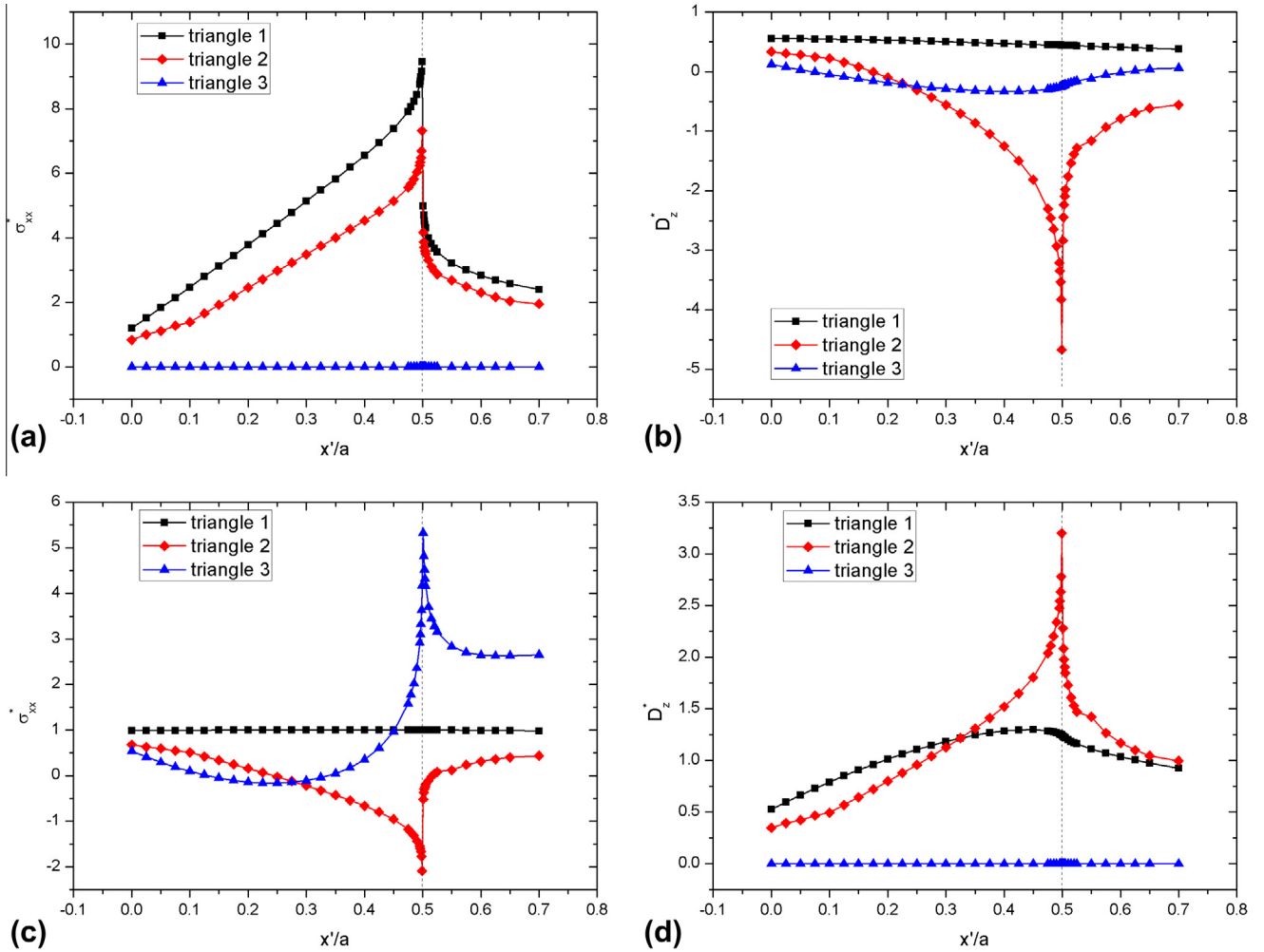
**Fig. 8.** Variation of dimensionless stress and electric displacement components along the local dimensionless coordinate $x'/a$: (a) variation of $\sigma_{xx}^*$ due to linear eigenstrain $\gamma_{Lm}^{*0} = 0, \gamma_{xx}^{*x} = \gamma_{zz}^{*x} = 0.07, \gamma_{Lm}^{*z} = 0$. (b) Variation of $D_z^*$ due to linear eigenstrain $\gamma_{Lm}^{*0} = 0, \gamma_{xx}^{*x} = \gamma_{zz}^{*x} = 0.07, \gamma_{Lm}^{*z} = 0$. (c) Variation of $\sigma_{xx}^*$ due to linear eigenstrain $\gamma_{Lm}^{*0} = 0, \gamma_{Lm}^{*x} = 0, \gamma_{xx}^{*z} = \gamma_{zz}^{*z} = 0.07$. (d) Variation of $D_z^*$ due to linear eigenstrain $\gamma_{Lm}^{*0} = 0, \gamma_{Lm}^{*x} = 0, \gamma_{xx}^{*z} = \gamma_{zz}^{*z} = 0.07$.

in $x(z)$. It is observed from these figures that, for triangle # 2 at the vertex A, the stress $\sigma_{xx}$ and electric displacement $D_z$ are both singular under linear eigenstrain in $x$ or $z$. For triangle # 1, stress $\sigma_{xx}$ shows a singularity at this vertex under linear eigenstrain in $x$, but it is regular under linear eigenstrain in $z$ (Fig. 8a vs. c). For triangle #3, stress $\sigma_{xx}$ exhibits singularity only under linear eigenstrain in $z$. Therefore, the geometric shape, embedded orientation, and eigenstrain distribution can strongly affect the singularity at the vertex of the polygonal QWR.

## 4. Conclusions

In this paper, we have derived an exact closed-form solution for the Eshelby problem of polygonal inclusion (or QWR) in an anisotropic piezoelectric half plane, with the final expression involving only elementary functions. The solution is applied to square, triangular, and rectangular QWRs within the GaAs (0 0 1) half-plane substrate. The induced piezoelectric fields are mostly affected by the free surface, depth of the QWR, and the graded eigenstrain distribution. Our numerical results also demonstrate the significant influence of the QWR shape on the induced fields. Furthermore, for a polygonal QWR, its geometrical shape, embedded orientation, and eigenstrain distribution can all affect the vertex singularity. All the numerical results can be served as benchmarks and could be

useful to the analysis of strained QWR structures of arbitrary shape with general anisotropic piezoelectricity.

## References

Andreev, A.D., Downes, J.R., Faux, D.A., O'Reilly, E.P., 1999. Strain distribution in quantum dots of arbitrary shape. J. Appl. Phys. 86, 297–305.

Chung, M.Y., Ting, T.C.T., 1996. Piezoelectric solid with an elliptic inclusion or hole. Int. J. Solids Struct. 33, 3343–3361.

Dong, C.Y., Lo, S.H., Cheung, Y.K., 2003. Stress analysis of inclusion problems of various shapes in an infinite anisotropic elastic medium. Comput. Methods Appl. Mech. Eng. 192, 683–696.

Eshelby, J.D., 1957. The determination of the elastic field of an ellipsoidal inclusion, and related problems. Proc. R. Soc. Lond. A241, 376–396.

Eshelby, J.D., 1961. Elastic inclusions and inhomogeneities. In: Sneddon, I.N., Hill, R. (Eds.), Progress in Solid Mechanics, vol. 2, North-Holland, Amsterdam, pp. 89–140.

Faux, D.A., Downes, J.R., O'Reilly, E.P., 1997. Analytic solutions for strain distribution in quantum-wire structures. J. Appl. Phys. 82, 3754–3762.

Freund, L.B., Gosling, T.J., 1995. Critical thickness for growth of strained quantum wires in substrate V-grooves. Appl. Phys. Lett. 66, 2822–2824.

Glas, F., 2002a. Analytical calculation of the strain field of single and periodic misfitting polygonal wires in a half-space. Philos. Mag. A82, 2591–2608.

Glas, F., 2002b. Elastic relaxation of isolated and interacting truncated pyramidal quantum dots and quantum wires in a half space. Appl. Surf. Sci. 188, 9–18.

Guo, L., Nie, G.H., Chan, C.K., 2011. Elliptical inhomogeneity with polynomial eigenstrains embedded in orthotropic materials. Arch. Appl. Mech. 81, 157–170.

Jiang, X., Pan, E., 2004. Exact solution for 2D polygonal inclusion problem in anisotropic magnetoelectroelastic full-, half-, and bimaterial-planes. Int. J. Solids Struct. 41, 4361–4382.

Ju, J.W., Sun, L.Z., 2001. Effective elastoplastic behavior of metal matrix composites containing randomly located aligned spheroidal inhomogeneities. Part I: micromechanics-based formulation. Int. J. Solids Struct. 38, 183–201.

Kouris, D.A., Mura, T., 1989. The elastic field of a hemispherical inhomogeneity at the free surface of an elastic half space. J. Mech. Phys. Solids 37, 365–379.

Li, S., Sauer, R., Wang, G., 2007. The Eshelby tensors in a finite spherical domain: I. Theoretical formulations. J. Appl. Mech. 74, 770–783.

Liu, L.P., 2010. Solutions to the periodic Eshelby inclusion problem in two dimensions. Math. Mech. Solids 15, 557–590.

Ma, H.M., Gao, X.L., 2011. Strain gradient solution for a finite-domain Eshelby-type plane strain inclusion problem and Eshelby's tensor for a cylindrical inclusion in a finite elastic matrix. Int. J. Solids Struct. 48, 44–55.

Mejak, G., 2011. Eshelby tensors for a finite spherical domain with an axisymmetric inclusion. Eur. J. Mech. A Solids 30 (4), 477–490.

Michelitsch, T.M., Gao, H., Levin, V.M., 2003. Dynamic Eshelby tensor and potentials for ellipsoidal inclusions. Proc. R. Soc. Lond. A459, 863–890.

Mura, T., 1987. Micromechanics of Defects in Solids, 2nd Revised ed. Kluwer Academic Publishers, Dordrecht.

Nie, G.H., Guo, L., Chan, C.K., Shin, F.G., 2007. Non-uniform eigenstrain induced stress field in an elliptic inhomogeneity embedded in orthotropic media with complex roots. Int. J. Solids Struct. 44, 3575–3593.

Nozaki, H., Taya, M., 1997. Elastic fields in a polygon-shaped inclusion with uniform eigenstrains. J. Appl. Mech. 64, 495–502.

Pan, E., 2002. Elastic and piezoelectric fields in substrates GaAs (001) and GaAs (111) due to a buried quantum dot. J. Appl. Phys. 91, 6379–6387.

Pan, E., 2004. Eshelby problem of polygonal inclusions in anisotropic piezoelectric full- and half-planes. J. Mech. Phys. Solids 52, 567–589.

Rahman, M., 2002. The isotropic ellipsoidal inclusion with a polynomial distribution of eigenstrain. J. Appl. Mech. 69, 593–601.

Ru, C.Q., 1999. Eshelby's problem of an inclusion of arbitrary shape in a plane or half-plane. J. Appl. Mech. 66, 315–322.

Ru, C.Q., 2003. Eshelby inclusion of arbitrary shape in an anisotropic plane or half-plane. Acta Mech. 160, 219–234.

Sharma, P., Sharma, R., 2003. On the Eshelby's inclusion problem for ellipsoids with nonuniform dilatational Gaussian and exponential eigenstrains. J. Appl. Mech. 70, 418–425.

Smith, D.L., 1986. Strain-generated electric fields in [111] growth axis strained-layer superlattices. Solid State Commun. 57, 919–921.

Sun, L.G., Xu, K.Y., Pan, E., 2012. Inclusion of arbitrary polygon with graded eigenstrain in an anisotropic piezoelectric full plane. Int. J. Solids Struct. 49, 1773–1785.

Wang, B., 1992. Three-dimensional analysis of an ellipsoidal inclusion in a piezoelectric material. Int. J. Solids Struct. 29, 293–308.

Wang, J., Chu, H.J., 2006. A perturbation theory for calculating strain distributions in heterogeneous and anisotropic quantum dot structures. J. Appl. Phys. 100, 053520.

Wang, X., Pan, E., 2010. Two-dimensional Eshelby's problem for two imperfectly bonded piezoelectric half-planes. Int. J. Solids Struct. 47, 148–160.

Willis, J.R., 1981. Variational and related methods for the overall properties of composites. Adv. Appl. Mech. 21, 1–78.

Yu, H.Y., Sanday, S.C., Chang, C.I., 1994. Elastic inclusion and inhomogeneities in transversely isotropic solids. Proc. R. Soc. Lond. A444, 239–252.

Zou, W.N., He, Q.C., Zheng, Q.S., 2011. General solution for Eshelby's problem of 2D arbitrarily shaped piezoelectric inclusions. Int. J. Solids Struct. 48, 2681–2694.

Zou, W.N., He, Q.C., Zheng, Q.S., 2012. Inclusions in a finite elastic body. Int. J. Solids Struct. 49, 1627–1636.

Zou, W.N., Pan, E., 2012. Eshelby's problem in an anisotropic multiferroic bimaterial plane. Int. J. Solids Struct. 49, 1685–1700.